https://doi.org/10.1093/plphys/kiad107 PLANT PHYSIOLOGY 2023: 192: 871–885

Plant Physiology®

Research Article

Two isoforms of Arabidopsis protoporphyrinogen oxidase localize in different plastidal membranes

Boris Hedtke,* Sarah Melissa Strätker, Andrea C. Chiappe Pulido and Bernhard Grimm

Humboldt-Universität zu Berlin, Institute of Biology/Plant Physiology, Philippstraße 13 (Building 12), Berlin 10115, Germany

*Author for correspondence: boris.hedtke@hu-berlin.de (B.H.)
The author responsible for distribution of materials integral to the findings presented in this article in accordance with the policy described in the Instructions for Authors (https://academic.oup.com/plphys/pages/General-Instructions) is Boris Hedtke.

Abstract

All land plants encode 2 isoforms of protoporphyrinogen oxidase (PPO). While PPO1 is predominantly expressed in green tissues and its loss is seedling-lethal in Arabidopsis (*Arabidopsis thaliana*), the effects of PPO2 deficiency have not been investigated in detail. We identified 2 *ppo2* T-DNA insertion mutants from publicly available collections, one of which (*ppo2-2*) is a knock-out mutant. While the loss of PPO2 did not result in any obvious phenotype, substantial changes in PPO activity were measured in etiolated and root tissues. However, *ppo1 ppo2* double mutants were embryo-lethal. To shed light on possible functional differences between the 2 isoforms, PPO2 was overexpressed in the *ppo1* background. Although the *ppo1* phenotype was partially complemented, even strong overexpression of PPO2 was unable to fully compensate for the loss of PPO1. Analysis of subcellular localization revealed that PPO2 is found exclusively in chloroplast envelopes, while PPO1 accumulates in thylakoid membranes. Mitochondrial localization of PPO2 in Arabidopsis was ruled out. Since Arabidopsis *PPO2* does not encode a cleavable transit peptide, integration of the protein into the chloroplast envelope must make use of a noncanonical import route. However, when a chloroplast transit peptide was fused to the N-terminus of PPO2, the enzyme was detected predominantly in thylakoid membranes and was able to fully complement *ppo1*. Thus, the 2 PPO isoforms in Arabidopsis are functionally equivalent but spatially separated. Their distinctive localizations within plastids thus enable the synthesis of discrete subpools of the PPO product protoporphyrin IX, which may serve different cellular needs.

Introduction

Tetrapyrrole synthesis (TPS) is a fundamental metabolic pathway found in almost all living organisms. In plants, it consists of a series of at least 25 enzymatic reactions and gives rise to chlorophylls as well as siroheme, heme, and phytochromobilin (Tanaka and Tanaka 2007). While chlorophyll is thought to be the major end-product of the branched pathway in photoautotrophic plant tissue, demand for different tetrapyrroles varies strongly, depending on the cell type and developmental stage considered (Tanaka and Tanaka 2007). Since most of the late tetrapyrrole intermediates absorb light, and are therefore potentially detrimental, their accumulation must be strictly controlled. Numerous regulatory circuits are involved in TPS. Indeed, control of the initial steps in 5-aminolevulinic acid (ALA) synthesis alone requires several feedback mechanisms. The rate-limiting step in TPS is catalyzed by glutamyl-tRNA reductase (GluTR), which is responsible for the first step in the synthesis of ALA. The activity, stability, and subplastidal localization of GluTR are regulated by multiple factors that serve to modulate the supply and allocation of ALA for chlorophyll and the other tetrapyrroles (Meskauskiene et al. 2001; Czarnecki et al. 2011; Wang et al. 2018; Richter et al. 2019). In plants, TPS takes place exclusively within plastids. While all reactions, from ALA formation to the synthesis of protoporphyrinogen IX (Protogen), are catalyzed by soluble proteins in the plastidal stroma; all of the following enzymes, starting with protoporphyrinogen oxidase (PPO), are associated with organellar

Received November 22, 2022. Accepted January 24, 2023. Advance access publication February 21, 2023

Open Access

membranes (Joyard et al. 2009). By extracting 6 electrons from Protogen, PPO forms protoporphyrin IX (Proto), the last common precursor of chlorophyll and heme synthesis. The genes that encode PPO in plants belong to the HemY family of oxygenic, FAD-containing enzymes (Kobayashi et al. 2014). HemY-type PPOs are targeted by several classes of inhibitors that are agronomically important as herbicides. By blocking substrate binding, these inhibitors cause rapid accumulation of Protogen. The latter is nonspecifically oxidized to Proto, which generates singlet oxygen in the presence of light, leading mainly to lipid peroxidation and, ultimately, to cell death (Jacobs et al. 1991; Lee and Duke 1994).

All embryophytic plants possess 2 HemY-type PPO enzymes, and phylogenetic analyses point to a gene duplication event early in the evolution of land plants (Kobayashi et al. 2014). Consequently, in angiosperms, the isoforms PPO1 and PPO2 share only 25% amino acid-sequence identity (Lermontova et al. 1997). However, based on crystal structures available for tobacco (*Nicotiana tabacum*) PPO2 (Koch et al. 2004), *Bacillus subtilis* (Qin et al. 2010), and *Homo sapiens* (Qin et al. 2011), the overall folding pattern is largely conserved, even over long phylogenetic distances within the HemY family.

Plant PPO1 is translocated into plastids via a cleavable transit peptide at the N-terminus of the preprotein (Lermontova et al. 1997). Knock-down of *PPO1* results in photodynamic lesions in tobacco antisense lines (Lermontova and Grimm 2006), while knock-out mutants in Arabidopsis are seedling-lethal (Zhang et al. 2014). The localization of PPO2 is less clear. Initial analyses in tobacco suggested that PPO2 accumulates in mitochondria (Lermontova et al. 1997). Indeed, dual targeting of PPO2 to mitochondria and chloroplasts has been described for spinach (*Spinacia oleracea*) (Watanabe et al. 2001) and corresponds with a specific N-terminal extension found in members of the *Amaranthaceae* family. This extended N-terminal region was suggested to confer dual targeting by alternative use of 2 in-frame initiation codons (Watanabe et al. 2001). However, in Arabidopsis, proteome studies have identified PPO2 as a constituent of the plastid envelope membrane (Joyard et al. 2009). While PPO2-deficient plants have not been investigated so far, recent reports on herbicide resistance specifically conferred by mutations in PPO2 have drawn renewed attention to this specific isoform (Porri et al. 2022).

In the present study, we characterized Arabidopsis *ppo2* mutants and analyzed the localization of the PPO2 protein. Based on the complementation of seedling-lethal *ppo1* plants by *PPO2*, we demonstrated that the 2 PPO isoforms are spatially separated within plastids and assessed the degree of functional equivalence between them.

Results

Numerous T-DNA insertion mutant lines were tested for *PPO2* knockdown or knockout mutations. Two lines (SALK_141571 and SAIL_841_G04) were confirmed to harbor T-DNA left-border (LB) sequences integrated into different sites within the 201-bp Intron 13 of AtPPO2 (Fig. 1A). Closer inspection of the integration site in the mutant *ppo2-1* (SALK_141571) localized the LB and right-border (RB) sequences of the integrated T-DNA at 65 and 55 bp, respectively, from the 3′ end of Exon 13. Hence, the insertion resulted in a small deletion in Intron 13. In the case of *ppo2-2* (SAIL_841_G04), analysis of the *PPO2*-specific sequences flanking the T-DNA also localized its LB to Intron 13, at a point 33 bp downstream of Exon 13 (Fig. 1B). Homozygous plants were identified for both *ppo2* mutant lines (Fig. 1C). Nevertheless, numerous attempts to amplify the sequence flanking the RB of the T-DNA in the *ppo2-2* line failed. Since the integrity of Exon 13 in this mutant was crucial for its further use in functional studies of PPO2, additional PCRs were performed on *ppo2-2* genomic DNA using 4 different primers (named I to IV; Fig. 1B) to pin down the precise insertion site of the RB (Fig. 1D). PCRs employing primers I and II failed to amplify specific fragments from *ppo2-2* genomic DNA, while control templates (Col-0 and *ppo2-1*) gave rise to the expected products (Fig. 1D, left panels). Since amplicons starting at primers III and IV are intact in *ppo2-2* (Fig. 1D, right panels), we concluded that the T-DNA insertion in this line had resulted in the deletion of at least 12 bp of Exon 13, in addition to the loss of 33 bp of Intron 13.

PPO2 transcript abundance in both *ppo2* T-DNA insertion lines was evaluated by reverse transcription quantitative PCR (RT-qPCR). While the T-DNA insertion in Intron 13 of line *ppo2-1* results in a 40% decrease in *PPO2* transcripts, no *PPO2* mRNA at all is detectable in *ppo2-2* (Fig. 1E). Transcript abundances of *PPO1* and selected key TPS genes (*HEMA1* encoding glutamyl tRNA reductase1 [GluTR1], *FC1*, and *FC2* for the 2 ferrochelatase isoforms, *PORB* for protochlorophyllide oxidoreductase B) were not affected in either of the *ppo2* mutants.

Protein levels were characterized by immunoblot analyses (Fig. 1F). Antisera raised against AtPPO2 revealed reduced amounts of the PPO2 protein in *ppo2-1*. In protein extracts of the *ppo2-2* mutant, no PPO2-specific signal was detected. Immunoblot analyses of TPS- and photosynthesis-related proteins revealed no substantial change in amounts of PPO1, GluTR1, FC2, PORB, or the light-harvesting complex protein B1 (LHCB1) in either of the *ppo2* mutants in comparison to wild type (Fig. 1F).

Since both genomic and expression analyses characterized *ppo2-2* as a knockout mutant, further characterization was focused on this line. Analyses of the tetrapyrrole intermediates Mg protoporphyrin IX (MgP), Mg protoporphyrin monomethyl ester (MME), and protochlorophyllide (Pchlide), as well as the end-products chlorophyll and heme, indicated no disturbance of the TPS pathway under standard growth conditions in *ppo2-2* (Fig. 1G). An accumulation of Proto was detected neither in the wild type nor in

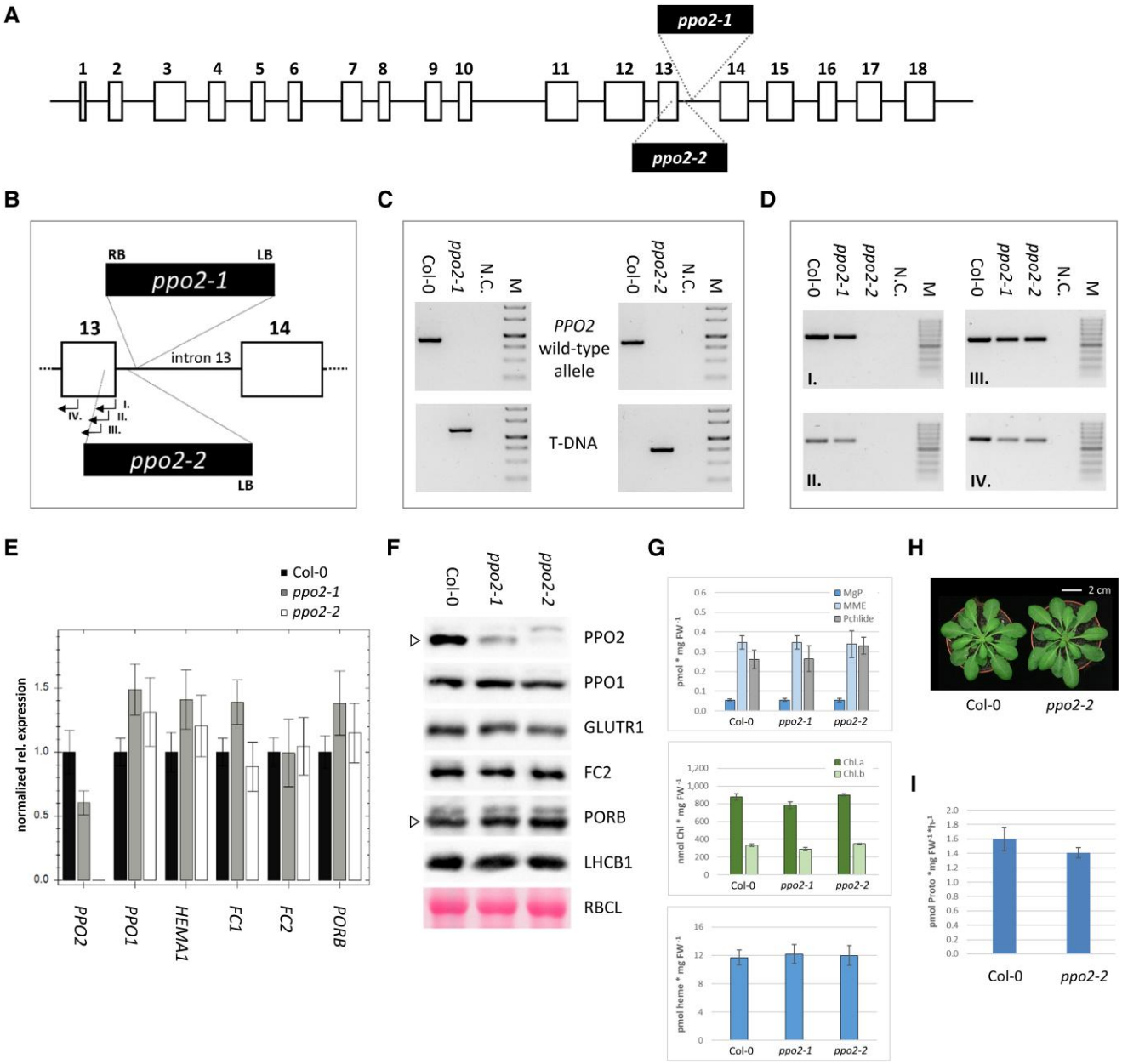

Figure 1. Characterization of Arabidopsis *ppo2* mutants. **A**) Structure of the Arabidopsis *PPO2* gene. Boxes and numbers indicate the exons of the coding region. **B**) Schematic depiction showing details of the insertions in Intron 13 in the mutants *ppo2-1* and *ppo2-2*. Sites of integration of LB and RB sequences are indicated by dashed lines. Exons 13 and 14 are boxed. Primers used for mapping *ppo2-2* (see **D**) are indicated by arrows and Roman numerals I to IV. **C**) Genotyping PCRs confirm the homozygosity of T-DNA insertions in *ppo2-1* and *ppo2-2*, respectively. Pairs of gene primers specific for the wild-type *PPO2* allele (upper panel) or a combination of gene- and LB-specific primers that amplify only *PPO2* alleles interrupted by T-DNA integration (lower panel) were used. **D**) PCR test of the integrity of the coding region of Exon 13 in *ppo2-2*. Four different primers that bind to sequences in Exon 13 (labeled I to IV; see also **B)** were used to map the deletion caused by T-DNA integration in *ppo2-2*. Wild-type (Col-0) and *ppo2-1* strains served as controls. Negative controls (N.C.) were performed without added DNA template. GeneRuler 1 kb **(C)** or 100 bp **(D)** DNA ladders (Thermo Scientific) were used as markers (M). **E**) Quantification of *PPO2*, *PPO1*, GluTR1 (*HEMA1*), *FC1*, *FC2*, and *PORB* transcripts in *ppo2* mutants relative to wild type. RT-qPCR data were normalized to SAND (At2g28390) transcript accumulation. Values are means ± SE ($n = 3$). Seedlings were cultivated for 14 d under SD conditions. **F**) Quantification of the PPO2 protein, selected tetrapyrrole pathway enzymes and light-harvesting complex protein LHCB1. As a reference, Ponceau-stained RBCL (RuBisCO large subunit) is depicted. Where antisera show cross-reactions, the specific band is marked by an open triangle. **G**) Quantification of TPS intermediates (Mg protoporphyrin IX [MgP], Mg protoporphyrin monomethylester [MME], protochlorophyllide [Pchlide]) and the end-products chlorophyll (shown as Chl.a and Chl.b) and heme (lower panel) in 2-wk-old *ppo2* mutants and the wild type. Values are means ± SD ($n = 4$). **H**) Phenotype of *ppo2-2* plants (bar = 2 cm) after 6 wk of cultivation under SD conditions. **I**) Comparison of PPO activity in leaf extracts of wild-type and *ppo2-2* mutant plants. Enzymatic activity is expressed as amount of Proto formed per time and FW of leaf material. The assay used 2-wk-old seedlings grown under SD conditions. Values are means ± SD ($n = 5$).

the *ppo2* mutants. Moreover, the visible phenotype of *ppo2-2* plants did not differ from wild type (Fig. 1H).

In order to evaluate the contribution of PPO2 to total plant PPO activity under photoautotrophic conditions, the level of PPO enzymatic activity in leaf extracts of *ppo2-2* was compared to that in wild-type samples. In 2-wk-old seedlings, total PPO activity in *ppo2-2* was reduced by 12% in comparison to Col-0 (Fig. 1I). This relatively minor impact of the loss of PPO2 on total plant PPO activity is in good agreement with relative transcript abundances described for the 2 PPO isoforms in Arabidopsis (Winter et al. 2007). In the majority of developmental stages, in green photoautotrophic tissue and in most plant organs, *PPO1* transcripts are clearly dominant over their *PPO2* counterparts.

Thus, in light of the markedly unequal contributions of the 2 isoforms to PPO activity, the divergent phenotypic consequences of the 2 knockout mutants are plausible. While loss of *PPO1* function is seedling-lethal (Zhang et al. 2014; Fig. 2A), the *ppo2-2* knockout mutant described here displays wild-type-like growth. Interestingly, *ppo1* plantlets also do not differ from wild type when cultivated under etiolating conditions (Fig. 2B). This suggests that PPO2 activity makes a larger contribution to TPS during germination and development in the dark.

To verify the more prominent role of PPO2 under these conditions, transcripts encoding both PPO isoforms were quantified in wild-type seedlings after 4 d of growth under etiolating conditions and during subsequent de-etiolation (Fig. 2C). Levels of *PPO1* transcripts during de-etiolation reveal light-inducible expression, which resembles that of both *HEMA1* and *FC2* (Fig. 2C). In contrast, amounts of *PPO2* mRNA are not substantially influenced by light. This difference in light-responsiveness between the 2 PPO isoforms was also observed at the protein level (Fig. 2D). While levels of PPO1 are clearly enhanced after 3 d of illumination, PPO2 abundance is less affected.

Due to the divergent responses of the PPO isoforms during de-etiolation, we also assessed the contribution of PPO2 to total PPO activity in dark-grown seedlings. In contrast to the minor decrease observed under photoautotrophic conditions (Fig. 1I), in vitro PPO activity is reduced by 88% in etiolated *ppo2-2* plantlets relative to wild type (Fig. 2E). In agreement with this marked decrease in *ppo2-2*, also a knockdown of *PPO2* expression in *ppo2-1* results in a reduced PPO activity in etiolated seedlings (Fig. 2E). Since these results obtained using dark-grown seedlings indicated a stronger contribution of PPO2 in nonphotoautotrophic tissues, PPO activity was also measured in roots of *ppo2-2* mutants. In comparison to wild-type tissue, *ppo2-2* roots revealed a 66% decrease in PPO activity (Fig. 2F).

Although the higher impact of PPO2 on overall PPO activity in etiolated seedlings and roots does not result in a visible phenotype, the results hint at a substantial contribution of *PPO2* during germination and early seedling growth. Moreover, since the *ppo1* mutant develops like the wild type in the dark (Fig. 2B), TPS during embryo and seed development is presumably supported predominantly by PPO2 function. To test this assumption, *ppo1ppo2* double mutants were generated. Crosses of heterozygous *ppo1* to homozygous *ppo2-2* enabled the identification of individuals heterozygous for *ppo1* and homozygous for *ppo2-2* (*ppo1/PPO1 ppo2/ppo2*) among the F2 offspring. These plants were phenotypically indistinguishable from wild type. However, analysis of seed development in ripening siliques revealed that around 25% of silique positions were empty. This corresponds to the expected number of seeds that were homozygous for the *ppo1ppo2* double mutation (Fig. 2G). No substantial abortion of seeds was observed in siliques of the heterozygous *ppo1* mutants or in homozygous *ppo2-2* mutants, i.e. the parental lines of the cross (Fig. 2G). The *ppo1* knockout mutant used in this study (GABI_539C07) harbors a T-DNA insertion in the C-terminal exon of *PPO1*, similar to *ppo1-2* (Li et al. 2019). PCR analyses confirmed the respective genotypes (Fig. 2H).

Overexpression of PPO2 complements *ppo1* only partially

Since PPO1 is the dominantly expressed isoform in light-exposed leaves, seedling lethality of *ppo1* is likely to be caused by a reduction in overall PPO activity that results in the accumulation of phototoxic Proto. To assess the functional equivalence of the 2 PPO isoforms, as well as the consequences of an increased contribution of PPO2 in green tissue, *PPO2* was expressed in the *ppo1* mutant background under the control of the *PPO1* promoter (*pPPO1*). Transformation of heterozygous *ppo1* mutants enabled the identification of BASTA-resistant T1 seedlings exhibiting enhanced *PPO2* expression in a heterozygous *ppo1* mutant background. Quantification of *PPO2* mRNA levels in 3 representative transgenic lines revealed a 5- to 10-fold increase in *PPO2* transcript levels compared to wild type, while amounts of the *PPO1* transcript were slightly reduced due to *ppo1* heterozygosity (Fig. 3A, lower left and middle). Since the *pPPO1:PPO2* DNA construct was designed to incorporate the untranslated regions (UTRs) of *PPO1* (upper scheme in Fig. 3A), RT-qPCR quantification using primers specific for the 3′UTR of *PPO1* included *PPO1* mRNA as well as transgenic *PPO2* transcripts, thus enabling quantitative comparisons of transgene expression with endogenous *PPO1* mRNA levels. The observed 5- to 10-fold increase in *PPO2* mRNA levels in the 3 depicted lines corresponded to an estimated 2-fold increase in amounts of the *PPO1* 3′UTR, when the slightly lower endogenous PPO1 expression is considered in heterozygous lines of the T1 offspring (Fig. 3A, lower right panel). Hence, as expected for expression under control of *pPPO1*, transgenic *PPO2* is expressed in similar amounts to wild-type *PPO1*.

Inspection of the T2 offspring of heterozygous *ppo1*(*pPPO1:PPO2*) individuals revealed seedlings with a deviating phenotype: about one-quarter of T2 seedlings displayed yellow-green cotyledons and true leaves in combination with retarded growth (Fig. 3B). Aberrant

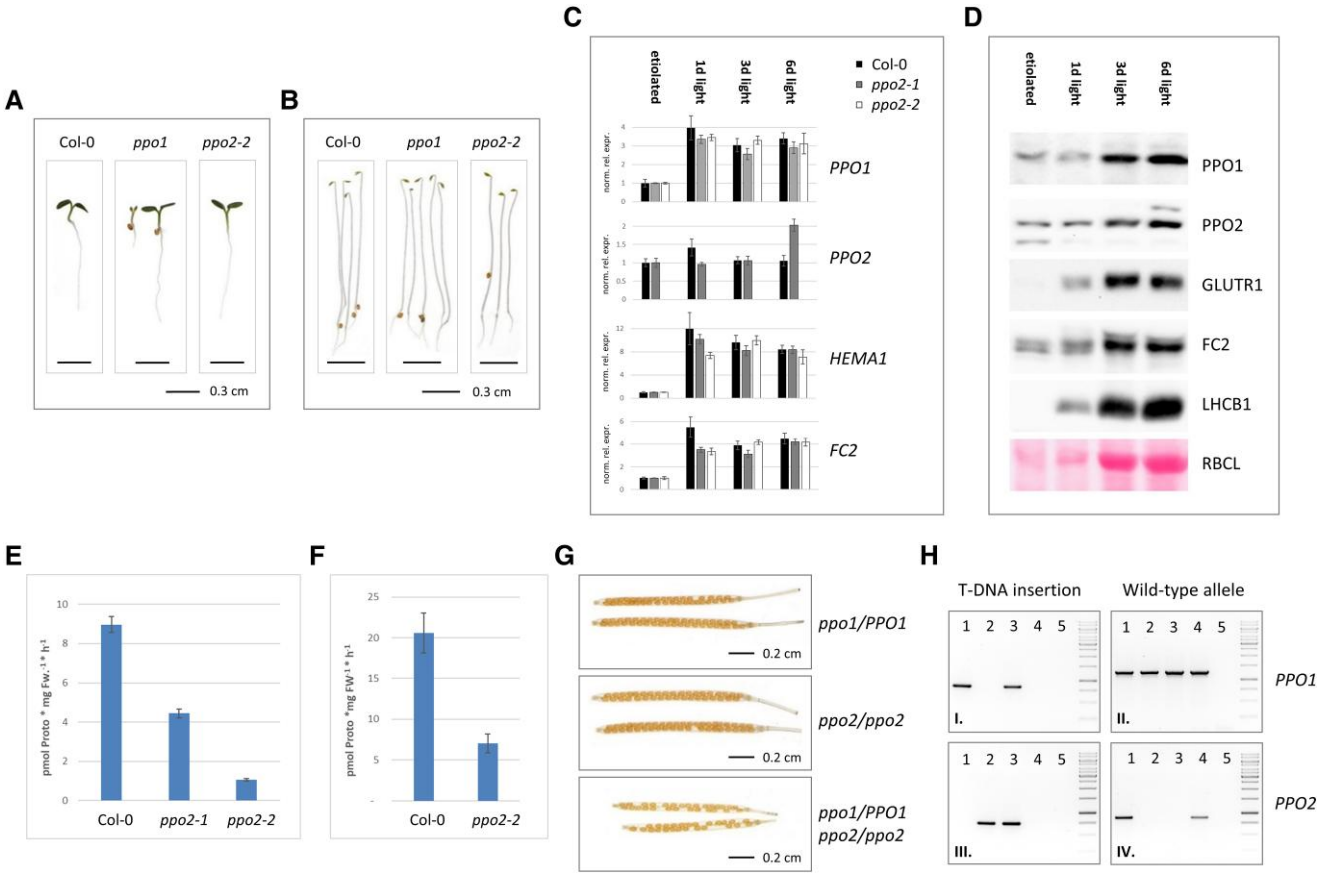

Figure 2. Contribution of the PPO2 isoform in etiolated seedlings, roots, and seed development. **A**) Comparison of wild-type and *ppo* mutant phenotypes after 4 d in continuous light (bar = 0.3 cm). *ppo1* seedlings were derived from a heterozygous parent and segregate. **B**) Wild-type and *ppo* mutant seedlings after 4 d growth in darkness (bar = 0.3 cm). **C**) Changes in accumulation of *PPO1*, *PPO2*, *HEMA1*, and *FC2* transcripts after exposure of 4-d-old etiolated seedlings to light for 1, 3, and 6 d. Analyses were performed for wild-type (Col-0), *ppo2-1*, and *ppo2-2* seedlings. Transcript abundance is given as normalized relative expression (norm. rel. expr.) relative to etiolated (=1) seedlings. Expression was normalized to accumulation of SAND (At2g28390) mRNA. Standard errors are indicated ($n = 3$). **D**) Immunoblot analysis of PPO1, PPO2, GluTR1, FC2, and LHCB1 levels during de-etiolation. The Ponceau-stained membrane (lower panel) depicts the accumulation of RuBisCO large subunit (RBCL) at the investigated time points. Protein samples represent identical amounts of fresh weight. **E**) PPO enzyme activity in etiolated wild type (Col-0), *ppo2-1*, and *ppo2-2* seedlings. Total extracts of seedlings grown for 4 d in darkness were used to quantify Proto formation in vitro. Values are means ± SD ($n = 3$). **F**) PPO enzyme activity in roots of wild type (Col-0) and *ppo2-2*. Roots were cut from seedlings grown for 15 d in continuous light on MS plates kept in a vertical position. Values are means ± SD ($n = 3$). **G**) Crosses of heterozygous *ppo1* mutants (*ppo1/PPO1*) to homozygous *ppo2*-2 plants (*ppo2/ppo2*) gave rise to *ppo1/PPO1 ppo2/ppo2* individuals in generation F2. Siliques formed by these plants show an abortion rate equivalent to approximately 25% of the developing seeds (lower panel). For comparison, siliques of the crossed lines are depicted in the upper panels (bar = 0.2 cm). **H**) Genotyping PCR analyses of plants whose seed formation is shown in (**G**). Plants heterozygous for *ppo1* (1), homozygous for *ppo2-2* (2), together with their *ppo1/PPO1 ppo2/ppo2* F2 siblings (3) are shown next to wild type (4) and nontemplate controls. Tests for inserted T-DNA in *PPO1* (I) and *PPO2* (III) are shown next to PCRs confirming the integrity of wild-type alleles of *PPO1* (II) and *PPO2* (IV). A DNA marker (GeneRuler 1 kb, ThermoFisher) is shown on the right.

pigmentation and growth were observed during the entire life cycle of these seedlings, as exemplified for 6-wk-old mutant seedlings in comparison to wild-type plants (Fig. 3C, left and middle). Following transfer of adult yellow-green mutant plants to continuous light, they flowered and set seeds. T3 siblings of such individuals displayed a uniform phenotype identical to that of their parental T2 plants.

Since expression of *PPO2* under the control of the *PPO1* promoter only partially complemented the *ppo1* phenotype, overexpression of *PPO2* was further increased by employing the cauliflower mosaic virus (CaMV) 35S promoter (p35S). The introduction of *p35S:PPO2* into the *ppo1* mutant background gave rise to transgenic individuals that complemented the *PPO1* knockout more effectively than lines harboring pPPO1:PPO2, but were still strongly perturbed in pigmentation and development in comparison to wild type (Fig. 3C, right). Transgenic lines expressing *p35S:PPO2* accumulated up to 100 times more *PPO2* transcript in comparison to wild type and similarly excessive amounts of PPO2 protein. Thus, the amounts of PPO2 in these lines exceeded the average PPO1 accumulation in wild type by more than an order of magnitude.

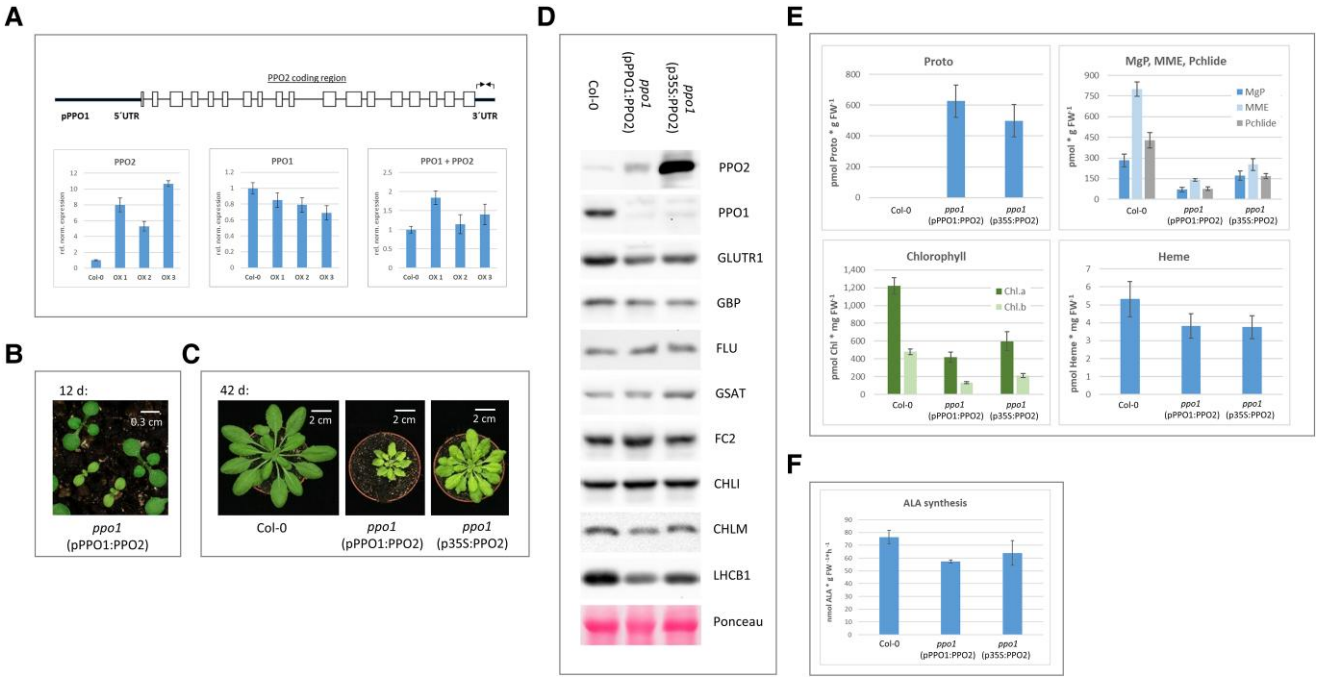

Figure 3. Overexpression of *PPO2* complements the *ppo1* phenotype only partially. **A**) Upper panel: Schematic depiction of the construct pPPO1:PPO2. Besides the *PPO1* promoter (pPPO1), the 5′UTR and the 3′UTR of *PPO1* (bold lines) flank the genomic sequence of *PPO2*. Exons are boxed. Primers specific for the 3′UTR of *PPO1* are indicated as arrows. Lower panel: RT-qPCR analysis of transgenic plants expressing pPPO1:PPO2. Three overexpressor lines (OX1-3) were analyzed in comparison to wild type (Col-0) for expression of *PPO2*, *PPO1* as well as the 3′UTR of *PPO1* ("PPO1 + PPO2"), which quantifies *PPO1* as well as the transgenic *PPO2*. Transcript abundance is given relative to wild type and was normalized using expression of SAND (At2g28390). Values are means ± SE ($n = 3$). **B**) Phenotypes of representative 12-d-old T2 seedlings of *ppo1* expressing with pPPO1:PPO2 (bar = 0.3 cm). The indicated genotype refers to the yellow-green smaller seedlings. **C**) Phenotype of *ppo1* mutants complemented by expression of PPO2 under control of *pPPO1* (middle) or *p35S* (right) in comparison to wild type (bar = 2 cm). All depicted individuals were grown for 6 wk under SD conditions. **D**) Immunoblot analysis of selected TPS enzymes (PPO1, PPO2, GluTR1, GBP, FLU, GSAT, FC2, CHLI, and CHLM) and light-harvesting proteins (LHCB1). The Ponceau-stained membrane depicts the accumulation of RBCL in the analyzed samples. **E**) Accumulation of tetrapyrrole intermediates (Protoporphyrin IX [Proto], Mg protoporphyrin IX [MgP], Mg protoporphyrin monomethylester [MME], protochlorophyllide [Pchlide]), and end-products (chlorophyll [Chl.a, Chl.b], heme). **F**) ALA-synthesizing capacity was determined in the presence of levulinate to inhibit ALAD activity. Analyses depicted in (**D**–**F**) were performed with mutant plants grown for 7 wk under SD conditions; similar-sized wild-type plants used for comparison were cultivated for 4 wk. Values in (**E**) and (**F**) are means ± SD ($n \geq 3$).

Homozygous *ppo1* mutants carrying the 2 different *PPO2* expression constructs were subjected to analyses of protein expression and the content of tetrapyrrole metabolites. Immunoblot analysis confirmed the yellow-green mutants as homozygous *ppo1* individuals overexpressing PPO2 to different extents (Fig. 3D). Immunoblot analyses of further TPS and LHC proteins revealed substantially reduced contents of GluTR1 and LHCB1 in *PPO2*-complemented *ppo1* plants (Fig. 3D). In contrast, amounts of the TPS enzymes GluTR-binding protein (GBP), FLUORESCENT (FLU), FC2, magnesium chelatase subunit I (CHLI), PORB, and magnesium-protoporphyrin IX methyltransferase (CHLM) were not altered in the partially complemented *ppo1* mutants (Fig. 3D). The partial rescue of *ppo1* was underlined by the analysis of TPS intermediates and end-products in the chlorotic mutants. The amount of Proto, which actually represents the sum of Protogen and Proto (owing to autooxidation of Protogen during sample extraction and processing), is strongly increased in both complemented lines, while downstream intermediates of the chlorophyll branch, such as MgP, MME, and Pchlide are strongly reduced (Fig. 3E). Chlorophyll contents are reduced by 50% to 70% in comparison to wild type, while the concentration of noncovalently bound heme corresponds to 73% of wild-type content, indicating that heme synthesis is less severely affected. The observed decrease in GluTR1 accumulation prompted us to compare ALA synthesis rates. A reduction of ALA synthesis by 18% to 25% was observed in the 2 complemented mutant lines relative to wild type (Fig. 3F).

Subplastidal localization of PPOs

As even excessive accumulation of PPO2 fails to fully complement the loss of PPO1 activity, the intracellular localization of the 2 PPO isoforms in Arabidopsis was re-examined. As PPO2 overexpression partially complements the seedling-lethality of *ppo1*, an exclusively mitochondrial targeting of PPO2 can be ruled out for Arabidopsis. To provide experimental evidence for the subcellular localization of

PPO2 in *Arabidopsis thaliana*, purified mitochondria, and chloroplasts were analyzed.

Firstly, mitochondria purified from wild-type *A. thaliana* plants were examined and selected proteins were analyzed on immunoblots (Fig. 4A). A strong increase in the signal intensity for the mitochondrial marker protein voltage-dependent anion-selective channel (VDAC), which belongs to a family of mitochondrial outer membrane porins, confirmed that the mitochondrial fraction had been successfully enriched (Fig. 4A). Nevertheless, PPO2 is detectable only in the total protein fraction. As expected, TIC110, a component of the translocon at the inner chloroplast (TIC) membrane complex, which served as a chloroplast marker protein, is strongly depleted in the mitochondrial fraction (Fig. 4A). To underline this finding, the experiment was repeated using transgenic Arabidopsis plants containing p35S:PPO2 to ensure that the protein is efficiently expressed (Fig. 4B). The organellar markers VDAC and TIC110 used as controls were distributed as in the wild type. PPO2 was strongly overexpressed, resulting in the presence of a weak PPO2-specific band in the mitochondrial fraction. However, comparison to the distribution obtained for TIC110 reveals that the mitochondrial fraction contains a contamination of chloroplasts. Residual impurities of plant mitochondrial preparations by plastidal or peroxisomal membranes are unavoidable and have been repeatedly described (Tran and Van Aken 2022).

Having excluded a mitochondrial localization for PPO2, the distribution of the 2 Arabidopsis PPO isoforms within plastids was addressed (Fig. 4C). Leaf chloroplasts were purified on Percoll gradients and, following hypotonic lysis, further separated into envelope and thylakoid fractions using sucrose-gradient ultracentrifugation. Immunoblot analysis revealed that PPO1 and PPO2 are differentially distributed in wild-type chloroplasts (Fig. 4C, left). While PPO1 is exclusively found in the thylakoid fraction, PPO2 accumulates specifically in envelope membranes. To verify the success of fractionation, proteins of known localization were detected in parallel (Fig. 4C). While TIC110 is a chloroplast envelope-specific protein, PORB is known to be enriched in thylakoid membranes. LHCB1 as an additional thylakoid marker is highlighted in the Ponceau staining pattern in Fig. 4C.

To validate the specificity of the observed PPO2 localization, the *ppo2-2* knockout mutant as well as an overexpression line were included in the analysis. When chloroplasts from *ppo2-2* plants were fractionated, no PPO2-specific immune signals were detected (Fig. 4C, middle). In contrast, plants overexpressing *PPO2* under the control of pPPO1 showed a wild-type-like distribution of PPO2, i.e. enrichment of the transgenic protein in the envelope fraction (Fig. 4C, right).

Comparison of PPO activities in purified chloroplasts and envelope fractions of wild-type Arabidopsis plants revealed a strong formation of Proto in the envelope-enriched fraction (Col-0 in Table 1). This high activity in purified envelopes reflects the minor contribution of envelopes to total chloroplast proteins: Since only about 1% to 2% of all chloroplast proteins are localized in the envelope (Douce and Joyard 1990), a specific enrichment of this fraction results in over-representation of envelope components when comparisons are normalized to protein amounts. As expected, the high level of envelope-localized PPO activity found in wild-type plants was not detectable in *ppo2-2* mutants (Table 1). PPO activity in whole isolated chloroplasts was also lower in *ppo2-2*. In addition, in vitro formation of Proto was investigated using plastidal fractions of *pPPO1:PPO2*-overexpressing plants. Here, a 12-fold increase in PPO activity was observed in purified chloroplasts, most of which was attributable to the envelope fraction (Table 1).

Arabidopsis PPO2 is strictly confined to the plastid envelope

The evidence for the specific localization of *A. thaliana* PPO2 in chloroplast envelope membranes presented above raised the question of the mechanism of its import. An N-terminally extended amino acid sequence was previously reported for spinach PPO2 (Watanabe et al. 2001). Among dicotyledonous plants, this amino-terminal extension is shared only by members of the *Amaranthaceae* family (shown for spinach and *Amaranthus palmeri* in Fig. 5A). Interestingly, it also seems to be a common feature of PPO2 isoforms in monocotyledonous plants (depicted for maize [*Zea mays*] and rice [*Oryza sativa*] in Fig. 5A). Like the vast majority of dicotyledonous PPO2 sequences, Arabidopsis PPO2 has a different and substantially shorter amino terminus, which resembles that of the tobacco PPO2 sequence (Fig. 5A). At5g14220, the gene encoding Arabidopsis PPO2, gives rise to a transcript containing a 5′ UTR of 58 nucleotides (At5g14220.1, Araport 11).

Interestingly, according to NTerdb (https://n-terdb.i2bc.paris-saclay.fr), a compilation of the results of targeted mass spectrometric analyses of the N-termini of mature *A. thaliana* proteins (Bienvenut et al. 2012), mature PPO2 begins with an acetylated alanine residue that is derived from the second amino acid of the annotated polypeptide (Fig. 5B). Since methionine excision and N-terminal acetylations are frequently observed cotranslational events (Giglione et al. 2015), the localization of PPO2 to chloroplast envelopes in Arabidopsis does not result from a canonical import event mediated by a cleavable transit peptide (Li and Teng 2013).

In contrast to the conflicting cellular localizations described for plant PPO2 isoforms in previous studies, data on organellar targeting of PPO1 are consistent. Plant PPO1 sequences harbor a characteristic chloroplast transit peptide and cleavage of 34 N-terminal amino acids has been confirmed in *A. thaliana* by mass spectrometric analysis (https://n-terdb.i2bc.paris-saclay.fr). The mature PPO1 protein is associated with thylakoid membranes (see Fig. 4C).

To investigate the degree of functional equivalence between the 2 Arabidopsis PPO isoforms, the cleavable transit peptide of PPO1 (TP^{PPO1}) was fused to the N-terminus of PPO2. The resulting gene construct encoding TP^{PPO1}PPO2

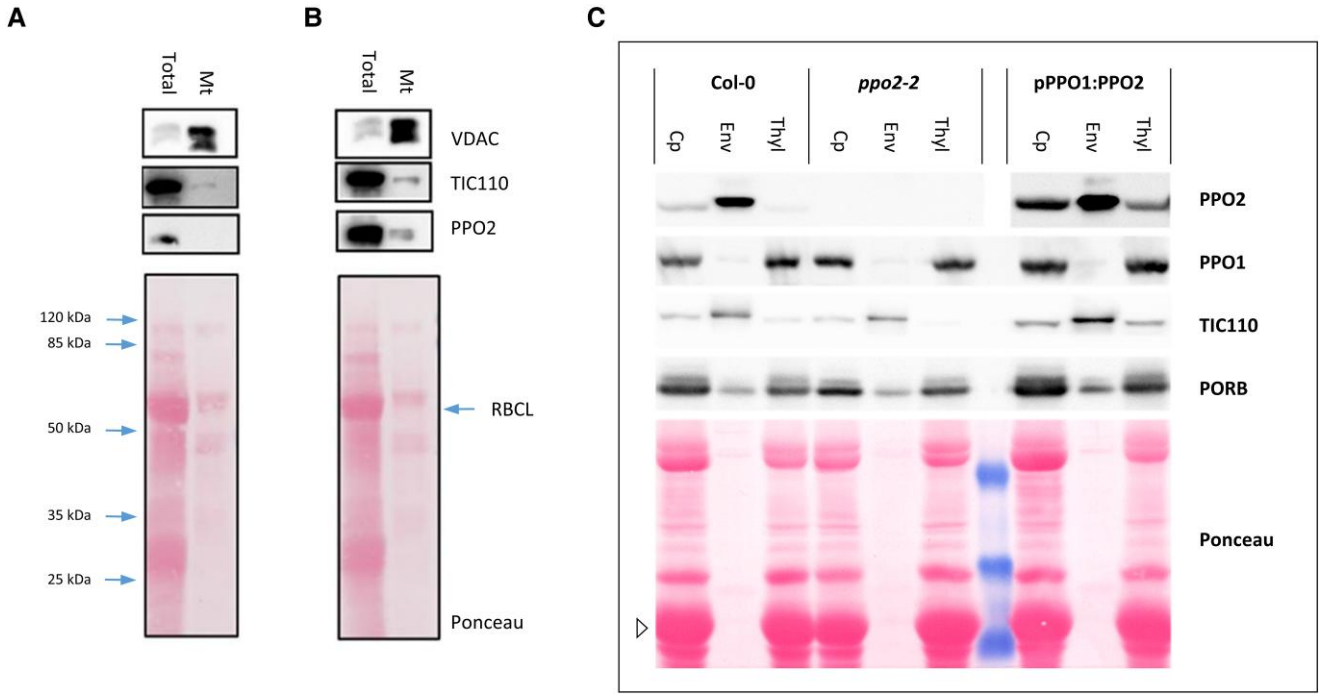

Figure 4. Localization of the 2 PPO isoforms of *A. thaliana* in different chloroplast membranes. Mitochondria were enriched from wild-type Col-0 **A)** and PPO2-overexpressing plants **B)**. Total leaf proteins (total) are loaded next to purified mitochondrial fractions (Mt). Immunoblot analyses were performed using antibodies directed against the mitochondrial VDAC, the chloroplast envelope protein TIC110 and PPO2. **C**) Percoll-purified chloroplasts (Cp) from Arabidopsis leaves were lysed hypotonically and used to enrich for plastidal envelopes (Env) and thylakoid (Thyl) membrane fractions by sucrose-density gradient ultracentrifugation. The analyses were performed using wild type (Col-0), PPO2 knockout mutants (*ppo2-2*), and plants expressing *PPO2* under the control of pPPO1 (pPPO1:PPO2). Immunoblots were incubated with antibodies specific for PPO2, PPO1, TIC110, and PORB. The depicted Ponceau-stained membrane includes prestained protein marker bands of 50, 35, and 25 kDa (blue). LHCB1 is indicated by an open triangle.

Table 1. PPO enzyme activity in chloroplast and envelope fractions

Plant line	Fraction	PPO activity (pmol Proto*min^{-1} *μg^{-1} protein)	Std. deviation (pmol Proto*min^{-1} *μg^{-1} protein)
Col-0	Purified Cp	0.67	0.17
	Envelope	29.61	1.19
ppo2-2	Purified Cp	0.33	0.03
	Envelope	0.30	0.28
pPPO1:PPO2 Overexpresser	Purified Cp	8.33	0.69
	Envelope	273.59	16.94

Purified chloroplasts (Cp) and envelope-enriched fractions from wild-type (Col-0), *ppo2-2*, and transgenic lines harboring pPPO1:PPO2 were used for in vitro PPO activity assays. Enzyme activities are given as Proto formed per protein and time unit. Standard deviations of 3 different measurements are indicated.

included the 37 amino-terminal residues of the PPO1 preprotein (Fig. 5C). Since the N-terminal methionine is absent in mature *A. thaliana* PPO2, it was omitted in the TP^{PPO1}PPO2 fusion in order to rule out an alternative initiation of translation. The newly generated *TP^{PPO1}PPO2* fusion gene was placed under control of *pPPO1* as well as *p35S* and transformed into the (heterozygous) *ppo1* mutant background.

Analyses of BASTA-resistant seedlings identified transformants homozygous for *ppo1* in the T1 generation. The phenotype of *ppo1*(*pPPO1:TP^{PPO1}PPO2*) plants was indistinguishable from wild type with regard to pigmentation and development, and clearly differed from the partial complementation observed in *ppo1*(pPPO1:PPO2) individuals (Fig. 5D). Interestingly, besides the complete complementation of *ppo1*, several of the *p35S:TP^{PPO1}PPO2* lines containing the stronger p35S promoter displayed necrotic lesions. Immunoblot analyses revealed the affected lines to represent the strongest overexpressors of the *TP^{PPO1}PPO2* fusions. Therefore, analyses presented here are based either on lines carrying pPPO1:TP^{PPO1}PPO2 or weaker expressors of p35S:TP^{PPO1}PPO2. Identical phenotypes were obtained when the chloroplast transit peptide of RBCS (the small subunit of ribulose bisphosphate carboxylase/oxygenase [RuBisCO]) was fused to PPO2 (TP^{RBCS}PPO2).

Purification of chloroplasts and subsequent separation of membrane fractions from transgenic lines harboring the chloroplast transit peptide fusion constructs revealed that both TP^{PPO1}PPO2 and TP^{RBCS}PPO2 accumulated primarily in the thylakoid fraction (Fig. 5E). Immunodetection of the chloroplast envelope protein DNAJD12 (At3g15110; Pulido and Leister 2018) and the LHCB1 signal on the

Ponceau-stained membrane proved a successful separation of envelope and thylakoid membranes. The sizes of the mature fusion proteins were similar to that of the overexpressed PPO2, indicating that the fused transit peptides were successfully removed.

Quantification of TPS intermediates and end-products by HPLC supported the full complementation of the mutant phenotype by *ppo1*(p35S:TP^{PPO1}PPO2) (Fig. 5F). In contrast to *ppo1*(p35S:PPO2), the accumulation of tetrapyrroles in homozygous *ppo1* plants expressing PPO2 fused to a cleavable chloroplast transit peptide is indistinguishable from that seen in wild-type plants (Fig. 5F). Thus, when fused to known chloroplast transit sequences, PPO2 is able to fully compensate for the loss of PPO1.

Discussion

Screening of publicly available T-DNA insertion lines identified 2 Arabidopsis *ppo2* mutants with either reduced (*ppo2-1*) or abolished (*ppo2-2*) *PPO2* expression. Neither of the mutants showed a visible phenotype when grown under standard conditions and quantification of in vitro PPO activity in total leaf extracts revealed only a small decrease in enzymatic activity in *ppo2-2* in comparison to wild type (Fig. 1).

While a knockout of *PPO1* has previously been shown to be seedling-lethal (Zhang et al. 2014), germination of segregating siblings of heterozygous *ppo1* mutants in the dark does not result in phenotypic differences (Fig. 2, A and B). This demonstrates that seed development, germination and etiolated growth do not essentially depend on PPO1 enzyme activity but can be adequately sustained by PPO2 alone. An evaluation of the individual contributions of both PPO isoforms during growth in darkness and subsequent de-etiolation based on the accumulation of *PPO1/2* transcripts and proteins (Fig. 2, C and D) indicated a stronger contribution of PPO2 under etiolating conditions and was confirmed by the highly reduced PPO activity in extracts of etiolated *ppo2* seedlings (Fig. 2E). A dominant impact of PPO2 on total PPO activity was also observed in root tissue (Fig. 2F). The embryo-lethal phenotype of the *ppo1ppo2* double mutant underlined the substantial contribution of PPO2 in early stages of plant development (Fig. 2G). However, apart from the drastic effects in double mutants, *ppo2-2* seedlings exhibit no visible phenotype. Hence, even complete loss of PPO2 can be adequately complemented by small amounts of PPO1, e.g. under etiolating conditions.

The observed ability to mutually compensate for the loss of the other PPO isoform, at least in nonphotoautotrophic tissue, raises the issue of the degree of functional overlap between PPO1 and PPO2 in Arabidopsis. Since the stronger expression of PPO1 in green tissue was hypothesized to represent the main obstacle for PPO2 to compensate the loss of PPO1, PPO2 was introduced into the *ppo1* mutant background under the control of the *PPO1* promoter. When the T2 offspring of heterozygous (*ppo1/PPO1*) T1 transformants were screened, about 25% of them turned out to be yellow green, slow-growing seedlings (Fig. 3B). Since the expression of *pPPO1:PPO2* did not fully complement *ppo1*, p35S:PPO2 lines were also generated. Resulting *ppo1(p35S:PPO2)* seedlings displayed improved complementation, but still failed to fully compensate for the loss of PPO1 (Fig. 3C). PPO2-complemented *ppo1* mutants were characterized by a strong accumulation of Proto, which, due to auto-oxidation, might represent either Protogen or Proto (Fig. 3E). In addition, the yellow-green phenotype was accompanied by reduced GluTR1 accumulation (Fig. 3D) and lower ALA synthesis rates (Fig. 3F). Since no other TPS proteins involved in ALA formation (GSAAT) or GluTR regulation (GBP, FLU) are affected (Fig. 3D), the observed decrease of ALA synthesis can be concluded to result from a specific effect of Proto(gen) accumulation on GluTR abundance.

Based on the inability of overexpressed PPO2 to fully complement *ppo1*, differences between the 2 Arabidopsis PPO isoforms were further elucidated by analyzing their subcellular localization.

Subcellular localization of PPO2

Lermontova et al. (1997) have previously described a mitochondrial localization for PPO2 in tobacco. Since the N-terminal region of Arabidopsis PPO2 closely resembles that of the *N. tabacum* isoform (Fig. 5A), we tested whether the former might also be targeted to these organelles. Mitochondria were purified from Arabidopsis wild-type and PPO2-overexpressing plants (Fig. 4, A and B). In both cases, no enrichment of PPO2 in the mitochondrial fraction was observed. Hence, a mitochondrial localization of Arabidopsis PPO2 can be ruled out.

Subsequent analyses of purified wild-type Arabidopsis chloroplasts enabled the subplastidal localization of PPO1 in thylakoid membranes (Fig. 4C) and demonstrated PPO2 to be strongly enriched in chloroplast envelope membranes. The specificity of the envelope localization of PPO2 was confirmed by experiments employing *ppo2-2* and *PPO2* overexpressor lines (Fig. 4C) and is supported by proteomic data (Froehlich et al. 2003; Ferro et al. 2010). Moreover, enzyme activity measurements revealed that conversion of Protogen in chloroplast envelope membranes depends specifically on PPO2, since the *ppo2-2* mutation effectively eliminated PPO activity from this fraction (Table 1).

The PPO1 distribution described here differs from data presented by Ferro et al. (2010), who reported the presence of PPO1 in both thylakoids and envelope membranes, based on mass spectrometric analyses. Since the applied fractionation by sucrose-gradient centrifugation enriches for envelope membranes which are largely free of contamination by thylakoids (see LHCB1 in Fig. 4C), the observed minor differences in the distribution of PPO1 require further investigation. In contrast, thylakoid membrane fractions obtained by sucrose density-gradient centrifugation still contain substantial amounts of envelope proteins (Matringe et al. 1992) (see TIC110 in Fig. 4C). Hence, an exclusive assignment of chloroplast membrane proteins to the envelope is more difficult to

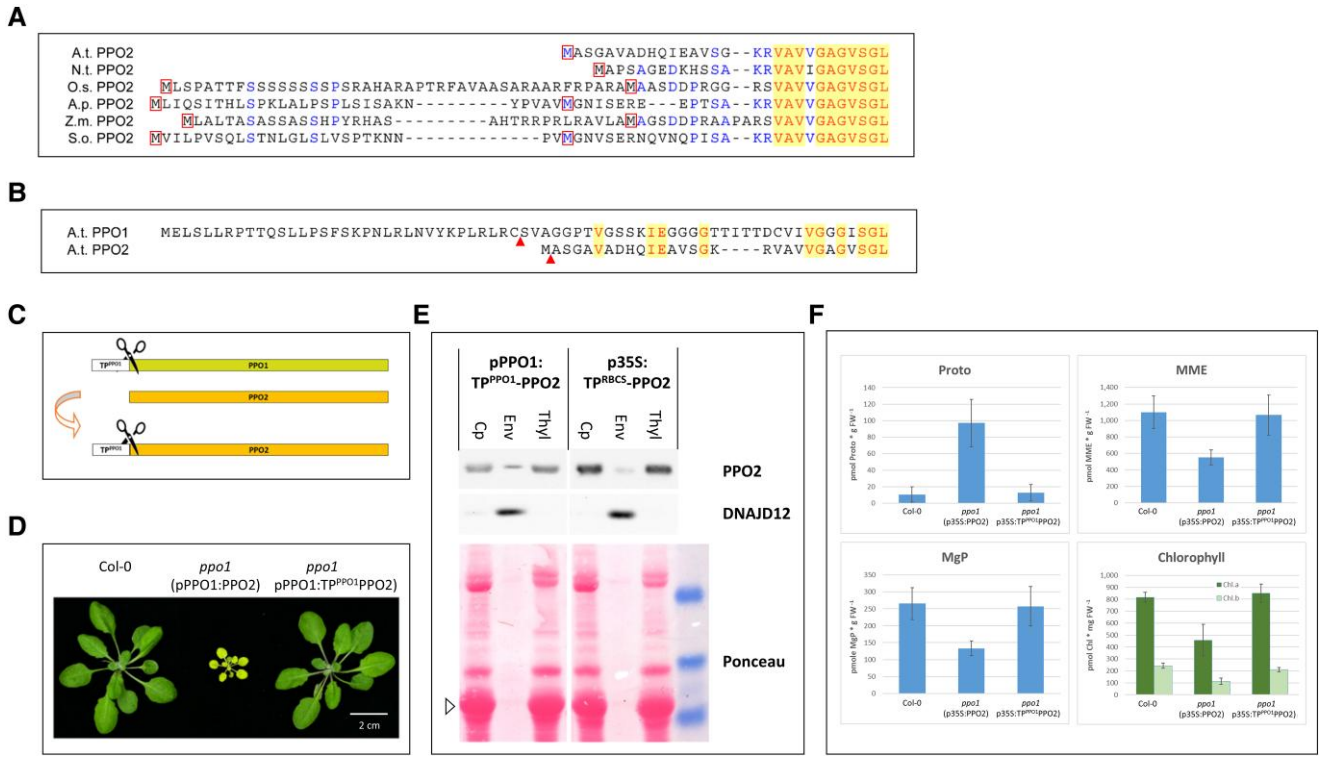

Figure 5. Targeting of PPO2 to thylakoid membranes enables full complementation of *ppo1*. **A**) Alignment of the N-terminal sequences of PPO2 proteins from representative angiosperms. In the majority of dicotyledonous plants, the N-terminus of PPO2 lacks a predicted cleavable transit peptide, as depicted for *A. thaliana* (A.t.) and *N. tabac*um (N.t.). In plants of the *Amaranthaceae* family, as shown here for *S. oleracea* (S.o.) and *A. palmeri* (A.p.), the N-terminal sequence is extended, as it is in monocotyledonous angiosperms such as *Z. mays* (Z.m.) and *O. sativa* (O.s.). Red boxes highlight methionine residues. Identical residues are shown in red font against a yellow background, similar amino acids are shown in blue. **B**) Alignment of the amino termini of PPO1 and PPO2 of Arabidopsis. N-termini of mature PPO proteins identified by mass spectrometry (using NTerdb) are indicated by red arrows. Identical amino acids are highlighted. **C**) Scheme illustrating the fusion of 37 N-terminal amino acids of A.t. PPO1 to AtPPO2 giving rise to TP^{PPO1}PPO2 which contains a cleavable transit peptide. **D**) Phenotypic comparison of wild-type and homozygous *ppo1* mutants complemented with pPPO1:PPO2 and pPPO1:TP^{PPO1}PPO2, respectively (bar = 2 cm). Plants were cultivated for 4.5 wk under SD conditions. **E**) Immunoblot analyses of purified chloroplasts (Cp) and fractions enriched for envelope (Env) and thylakoid (Thy) membranes of Arabidopsis plants expressing pPPO1:TP^{PPO1}PPO2 and p35S:TP^{RBCS}PPO2, respectively, in the Col-0 background. Antisera specific for PPO2 and DNAJD12 were used. The lower panel depicts the Ponceau-stained membrane, marker bands of 50, 35, and 25 kDa are included at the right side. LHCB1 is highlighted by an open triangle. **F**) HPLC analyses of *ppo1* complemented with either envelope- (p35S:PPO2) or thylakoid-targeted (p35S:TP^{PPO1}PPO2) PPO2 constructs. The tetrapyrrole intermediates Protoporphyrin IX (Proto), Mg protoporphyrin IX (MgP), Mg protoporphyrin monomethylester (MME) as well as chlorophyll (Chl.a, Chl.b) were quantified in 3.5-wk-old wild-type and complemented mutant seedlings. Mean values and SD ($n \geq 3$) are indicated.

prove conclusively and requires additional, independent evidence (see below).

The N-terminus of Arabidopsis PPO2 is typical for the majority of PPO2 sequences in dicotyledonous plants. It lacks a cleavable transit peptide, as illustrated by sequence alignments revealing highly conserved amino acids starting with a serine at Position 15 (Fig. 5A). Cleavable transit peptides are characterized by low sequence conservation, and typically vary in length between 20 and 150 residues (Balsera et al. 2009). Indeed, the identification of mature N-termini of Arabidopsis proteins has revealed that PPO2 begins with an acetylated alanine at Position 2 (https://n-terdb.i2bc.paris-saclay.fr).

Interestingly, a small group of dicotyledonous plants (*Amaranthaceae*, see spinach and *A. palmeri* in Fig. 5A), as well as all monocotyledonous plants (maize and barley in Fig. 5A), encode PPO2 isoforms with a distinct N-terminal extension showing characteristics of a cleavable transit peptide. Since several gene annotations have been published for Arabidopsis PPO (Araport 11; Cheng et al. 2017) the possibility of a similar N-terminal extension of PPO2 must be considered. At5g14220.4 comprises a hypothetical, prolonged PPO2 reading frame with 2 potential start codons, respectively, situated 138 and 144 bp upstream of the translation initiation site referred to in this study and described by the initial gene model At5g14220.1. However, we attribute no functional relevance to these upstream ATG codons for the following reasons. First, no PCR amplification of the putative *PPO2* transcripts situated upstream of the annotated 58 bp of 5′ UTR was possible. Secondly, mapped Arabidopsis transcription start sites (Nielsen et al. 2019) confirm that PPO2

transcripts initiate within the annotated 5′UTR of model At5g14220.1. Thirdly, the findings reported in this study based on *PPO2* overexpression initiating at the annotated *PPO2* start codon (At5g14220.1, Fig. 5A) agree with the changes observed in plastid envelopes of *ppo2-2* knockout mutants (Fig. 4C and Table 1). In addition, the exclusive accumulation of PPO2 in chloroplast envelope fractions in wild-type *A. thaliana* strongly suggests that no differently targeted PPO2 variants are present in Arabidopsis.

Targeting of PPO2 to thylakoids results in full complementation of *ppo1*

The clearly distinctive subplastidal localizations of the 2 Arabidopsis PPO isoforms can in principle account for the inability of overexpressed PPO2 to complement the *ppo1* mutant. However, given that the proteins share only 25% sequence identity, a functional equivalence of both isoforms is not a matter of course. To elucidate the ability of PPO2 to fully substitute PPO1 function, the N-terminal methionine of PPO2 was replaced by the PPO1 transit peptide sequence to enable it to be targeted to thylakoids (Fig. 5, B and C). Resulting complemented *ppo1*(pPPO1:TP^{PPO1}PPO2) plants exhibited no phenotypic differences to wild type (Fig. 5D), illustrating the ability of TP^{PPO1}PPO2 to fully compensate for the loss of PPO1 (Fig. 5F). *ppo1*(pPPO1:TP^{PPO1}PPO2) lines also demonstrate that even low amounts of thylakoid-targeted PPO2 resulting from expression under control of pPPO1 are sufficient to fully complement *ppo1*. Since a comparable complementation using PPO2 was not even achieved in p35S-based overexpressors, the targeting of *A. thaliana* PPO2 to the chloroplast envelope can be deduced to be highly specific.

Although not experimentally addressed in the present study, PPO2 is assumed to be located at the inner membrane of chloroplast envelope. Its substrate is provided by soluble stromal CPO1, while Proto is further processed by chelatases localized inside the chloroplast. Hence, assuming that PPO2 is an inner envelope membrane-bound protein without a cleavable transit peptide, its targeting is hypothesized to occur via a noncanonical mode of integration previously described for plastidal inner envelope membrane proteins, such as chloroplast envelope quinone oxidoreductase (ceQORH) and inner envelope protein 32 (IEP32) (Miras et al. 2002; Nada and Soll 2004). For ceQORH, an internal sequence motif has been reported to be responsible for envelope integration (Miras et al. 2007).

Physiological impact of the separate subplastidal localization of PPO2

A spatial separation of plant TPS at the level of Proto formation into an thylakoid-bound and an envelope-bound part has been postulated earlier (reviewed in Mochizuki et al. 2010). Intriguingly, differing PPO localizations establish an additional regulatory layer in TPS by giving rise to separate Proto pools within plastids. Our study demonstrates that the spatial separation of PPO enzyme activities in Arabidopsis results from envelope-specific targeting of the PPO2 isoform. In addition, the only partial complementation observed in Arabidopsis *ppo1*(p35S:PPO2) plants indicates that Proto synthesized at the envelope is not accessible to thylakoid-localized chelatases and thus supports the idea of separate plastidal Proto pools.

The main PPO activity in leaf tissue is based on thylakoid membrane-localized PPO1 and hypothesized to deliver Proto for chlorophyll as well as for plastidal heme synthesis. This coincides with the presence of MgCh and downstream enzymes of the chlorophyll branch as well as with the thylakoid-specific localization of the dominant ferrochelatase isoform FC2 in this plastidal subcompartment (Joyard et al. 2009). However, also PPO2-based, envelope-specific Proto synthesis contributes substantially to total PPO activity in leaves. It is tempting to speculate that envelope-specific Proto formation is linked to requirement for extraplastidal heme, which has been related to the FC1 isoform in Arabidopsis (Scharfenberg et al. 2015; Woodson et al. 2015; Fan et al. 2019). The exclusion of mitochondrial targeting of PPO2 reported here for Arabidopsis implies that heme is exclusively synthesized in plastids. Future analyses will provide further insights into specific protein interactions of the PPO isoforms and shed additional light on the importance of the spatial differentiation for plant TPS.

The assignment of plant PPO2 to the inner envelope membrane of the chloroplast is also of economic and biotechnological relevance. PPO2 has recently attracted attention for several reported cases of resistance against PPO-inhibiting herbicides which are caused by PPO2 point mutations (Porri et al. 2022). Such sequence variations have been discovered repeatedly in *Amaranthus* species, in which the N-terminal region of PPO2 (and thus its subcellular distribution) differs from that found in Arabidopsis (Fig. 5A). The recent description of an obviously lethal phenotype caused by severe *PPO2* mutations in *Amaranthus* (Porri et al. 2022) deviates from the Arabidopsis *ppo2-2* phenotype described in this study and hints at fundamental differences in PPO2 function between *Amaranthaceae* and dicots encoding Arabidopsis-type PPO2 sequences.

In summary, the data presented here are an attractive starting point for the re-evaluation of the role of PPO2 in TPS in angiosperms. It is important to explore the individual contributions of both PPO isoforms to the pathway during plant development up to seed formation, as well as in different tissues and organs. Based on the strong impact of Arabidopsis *ppo2-2* on PPO enzyme activity in etiolated tissue and roots, further dissection of the function and subplastidal localization of the 2 PPO isoforms in nonphotosynthetic plastids will be of particular interest.

Materials and methods

Plant material and growth conditions

The Arabidopsis (*A. thaliana*) genotypes used included the wild type (Col-0), *ppo1* (GK_539C07), *ppo2-1* (SALK_141571),

and *ppo2-2* (SAIL_841_G04). Plants were grown on soil at 23°C and 100 μmol photons m^{-2} s^{-1} under short-day (SD) conditions (10 h light, 14 h dark). Seeds used for etiolated growth were stratified for 3 d at 4°C, followed by light induction for 5 h at 23°C. Etiolated seedlings were grown for 4 d at room temperature (RT) either on plates containing Murashige and Skoog medium (4.4 g L^{-1} Murashige and Skoog, 0.05% [w/v] 2-(N-morpholino)ethanesulfonic acid, 0.8% [w/v] agar, pH 5.7) or on soil-filled pots covered with gauze.

Genotyping PCRs

ppo2-1 and *ppo2-2* mutants were tested for T-DNA insertions in *PPO2* using the primer pairs PPO2R2/pROK_LB4 and PPO2R2/Garlic_LB, respectively. The presence of wild-type *PPO2* alleles was analyzed in both lines using PPO2F2/PPO2R2. Primer walking used to localize the insertion event in *ppo2-2* employed Primers I–IV, in combination with PPO2F3. Analyses of the *ppo1* mutant were performed with the primers PPO1 down fw/Gabi LB (T-DNA) and AtPPO1_genot.WtFw/AtPPO1_genot.WtRv (wt allele). Primer sequences used are listed in Supplemental Table S1.

Cloning

The primer combinations PPO1_Promoter_FW_SacI/PPO1_5′UTR_RV_fusion and PPO1_3′UTR_FW_fusion/PPO1_3′UTR_RV_PmlI were used to amplify the *PPO1* promoter and 3′UTR, respectively, from wild-type *A. thaliana* DNA. The 2 fragments were fused using the outer primers, and cloned into pJET (Thermo Scientific). The insert was then transferred into the binary vector pCAMBIA 3,301 (Cambia, Canberra, Australia) using SacI and PmlI, thus giving rise to pCAM_PPO1, in which the *PPO1* promoter and 3′UTR are separated by AscI and SbfI restriction sites. The wild-type Arabidopsis *PPO2* was amplified as a 3.8-kb genomic fragment using PPO2_FW_AscI/PPO2_RV_SbfI, and ligated into AscI/SbfI-cleaved pCAM_PPO1, resulting in pPPO1:PPO2. To generate p35S:PPO2, *PPO2* was amplified using PPO2_FW_SacI/PPO2_RV_SacI, and ligated into pGL1 (Apitz et al. 2014) after restriction with SacI.

DNA fragments encoding the 37 N-terminal amino acids of PPO1 and PPO2 (lacking the initial methionine) were amplified using the primer pairs PPO1_FW_SacI/P1P2_Fusion_RV and P1P2_Fusion_FW/PPO2_RV_SacI, respectively. Subsequent fusion of the fragments was achieved by annealing and amplification using the outer SacI primers. The product was transferred into pGL1 via SacI cloning and yielded p35S:TP^{PPO1}PPO2. Alternatively, the fusion was reamplified using PPO1_FW_AscI/PPO2_RV_SbfI and inserted into pCAM_PPO1 cleaved with AscI and SbfI, resulting in pPPO1:TP^{PPO1}PPO2.

Fusion of PPO2 to the transit peptide of RBCS was achieved by amplification with RbcS_FW_PmlI/RbcsP2_Fusion_RV and RbcsP2_Fusion_FW/PPO2_RV_SacI. A fusion PCR utilizing outer PmlI/SacI primers and subsequent cloning into SmaI/SacI-cut pGL1 resulted in p35S:TP^{RBCS}PPO2.

RT-qPCR

RNA was extracted from frozen plant material homogenized in a mixer mill MM 400 (Retsch, Germany) using the citric acid protocol (Oñate-Sánchez and Vicente-Carbajosa 2008). Total RNA (1 μg) was transcribed following DNase I treatment using Moloney Murine Leukemia Virus reverse transcriptase and an oligo dT(18) primer according to the manufacturer's protocol (ThermoFisher Scientific). RT-qPCR analysis was carried out in a CFX96-C1000 96-well plate thermocycler (Bio-Rad, CA) using ChamQ Universal SYBR qPCR master mix (Vazyme). Calculation of gene expression levels was performed with the Bio-Rad CFX-Manager Software 1.6 using the $2^{-\Delta\Delta C(t)}$ method. Transcript accumulation was normalized using *SAND* (AT2G28390; Czechowski et al. 2004).

Protein extraction and western blot procedures

Total leaf protein was extracted from homogenized leaf material using 10 μL of 2× Laemmli buffer (Sambrook 2001) per mg fresh weight (FW). Samples were heated for 5 min at 95°C, centrifuged for 5 min (16,000 × *g*, RT). Samples representing either identical FW (1 mg) or adjusted to Chl/protein content were fractionated by electrophoresis on SDS-polyacrylamide gels (12% [w/v]) and blotted onto nitrocellulose membranes (Amersham Protran, GE Healthcare, United Kingdom). Membranes were stained with Ponceau S and probed with protein-specific antibodies according to Sambrook (2001). Polyclonal antisera against His-tagged recombinant Arabidopsis proteins GluTR1, GBP, FLU, PPO2, FC2, CHLI, CHLM, PORB, and DNAJD12 as well as *N. tabacum* PPO1 were raised in the authors' laboratory and affinity-purified using the antigen when necessary. Sera specific for LHCB1.6 and TIC110 were purchased from Agrisera (Sweden).

HPLC analyses

Tetrapyrroles were extracted from homogenized leaves using 300 μL of acetone:0.2 M NH_4OH (9:1), incubated for 30 min at −20°C and centrifuged for 30 min (16,000 × *g*, 4°C). The supernatant was analyzed by HPLC for (Mg) porphyrins and Chls. Noncovalently bound (ncb) heme was extracted from the remaining pellet by resuspension in 200 μL AHD (acetone:HCl:DMSO, 10:0.5:2) and incubated for 15 min at RT. After centrifugation for 15 min (16,000 × *g*, RT), the amount of ncb heme in the supernatant was quantified by HPLC. HPLC analyses were performed on Agilent LC systems following the methods described in Richter et al. (2019), using authentic standards for peak quantification.

Purification of organelles

Chloroplasts were purified from 6-wk-old Arabidopsis plants grown under SD conditions. Aliquots (20 g) of leaf material were homogenized in 450 mM sorbitol, 20 mM Tricine,

10 mM EDTA, 10 mM $NaHCO_3$, and 0.1% (w/v) BSA (pH 8.4) using a modified Waring blender (Kannangara et al. 1977). The homogenate was filtered through Miracloth and pelleted for 8 min at 500 × *g*. Following careful resuspension with a soft brush in RB (300 mM sorbitol, 20 mM Tricine, 2.5 mM EDTA, 5 mM $MgCl_2$, pH 8.4), the suspension was loaded on a step gradient of 40% and 80% Percoll in RB. Centrifugation for 30 min at 6,500 × *g* in a swing-out rotor enriched for intact chloroplasts at the Percoll interphase. Chloroplasts were carefully transferred, diluted in RB and pelleted for 6 min at 3,800 × *g*. Purified chloroplasts were lysed hypotonically in HLB (25 mM HEPES–KOH, pH 8.0) supplemented with protease inhibitor cocktail (Hycultec, Germany). Following incubation on ice for 1 h, 0.7 volumes of a mixture containing 0.6 M sucrose, 25 mM HEPES–KOH (pH 8.0), and 4 mM $MgCl_2$ were added and loaded on a sucrose step gradient consisting of 0.4, 1.0 and 1.2 M sucrose, each in 25 mM HEPES–KOH (pH 8.0). Ultracentrifugation at 200,000 × *g* for 1 h in a swing-out rotor enriched for chloroplast envelopes at the interphase between 0.6 and 1.0 M sucrose, while thylakoids formed a tight pellet. The latter was resuspended in HLB, while envelope membranes were transferred, washed in HLB, and collected by centrifugation at 48,000 × *g* for 1 h.

Mitochondria from 20 g of Arabidopsis leaves were isolated by intense homogenization in a modified Waring blender in EB (0.3 M sucrose, 25 mM K-pyrophosphate, 2 mM EDTA, 10 mM KH_2PO_4, 1% [w/v] PVP-40, 1% [w/v] BSA, 5 mM cysteine, pH 7.5). Following filtration through Miracloth, the plant debris was extracted 2 times by grinding in a mortar for 10 min with additional EB. The filtrates were then combined and centrifuged (5 min, 1,700 × *g*). The supernatant was centrifuged again (10 min, 20,000 × *g*), and the pellet was resuspended in WB (0.3 M sucrose, 10 mM MOPS, 1 mM EDTA, pH 7.2) and homogenized in a Potter–Elvejhem homogenizer. Dilution in WB was followed by centrifugation at 2,500 × *g* for 10 min. The supernatant was then pelleted again (10 min, 20,000 × *g*). The crude mitochondrial fraction was resuspended in WB and loaded onto a step gradient consisting of 18%, 25%, and 50% (v/v) Percoll in MGB (0.3 M sucrose, 10 mM MOPS, pH 7.2). Centrifugation at 40,000 × *g* for 45 min enriched the mitochondria on top of the 50% Percoll phase. Four final washes in WB at 20,000 × *g* for 10 min each were applied to obtain purified mitochondria.

PPO activity assays

Plant material was either homogenized under liquid N_2 in a mixer mill MM 400 (Retsch, Germany) or obtained from organelle purifications and dissolved in assay buffer (AB) containing 0.5 M Bis–Tris pH 7.5, 4 mM DTT, 2.5 mM EDTA, and 0.004% (v/v) Tween on ice. Aliquots (50 μL) of the extract were mixed with 150 μL of AB containing 4 μM Protogen at RT, and Proto formation was recorded over a period of 20 min on a Hitachi F-700 fluorescence spectrophotometer (excitation 405 nm, emission 635 nm). Conversion of relative fluorescence values is based on an authentic Proto standard dissolved in AB.

Accession numbers

Sequence data from this article can be found in the GenBank/EMBL data libraries under accession numbers *PPO1* At4g01690; *PPO2* At5g14220.

Acknowledgments

The excellent technical assistance of Kersten Träder is gratefully acknowledged. Sharhzad Grundler, Jana Sarrazin, and Florian Salisch contributed to the study during their students' projects. We are thankful to Paul Hardy for critical reading of the manuscript. Protogen for PPO activity assays was kindly provided by BASF (Germany).

Author contributions

B.H. and B.G. designed the research; B.H., A.C.C.P., and S.M.S. performed the experiments. B.H. and B.G. wrote the paper.

Supplemental data

The following materials are available in the online version of this article.

Supplemental Table S1. List of oligonucleotides used in the present study

Funding

We acknowledge the support by the German Academic Exchange Service (DAAD) to A.C.C.P.

Conflict of interest statement. The authors declare that there is no conflict of interest.

References

Apitz J, Schmied J, Lehmann MJ, Hedtke B, Grimm B. GluTR2 complements a hema1 mutant lacking glutamyl-tRNA reductase 1, but is differently regulated at the post-translational level. Plant Cell Physiol. 2014:**55**(3):645–657. https://doi.org/10.1093/pcp/pcu016

Balsera M, Soll J, Bolter B. Protein import machineries in endosymbiotic organelles. Cell Mol Life Sci. 2009:**66**(11–12):1903–1923. https://doi.org/10.1007/s00018-009-8644-2

Bienvenut WV, Sumpton D, Martinez A, Lilla S, Espagne C, Meinnel T, Giglione C. Comparative large scale characterization of plant versus mammal proteins reveals similar and idiosyncratic N-alpha-acetylation features. Mol Cell Proteomics. 2012:**11**(6): M111.015131. https://doi.org/10.1074/mcp.M111.015131

Cheng C-Y, Krishnakumar V, Chan AP, Thibaud-Nissen F, Schobel S, Town CD. Araport11: a complete reannotation of the *Arabidopsis thaliana* reference genome. Plant J. 2017:**89**(4):789–804. https://doi.org/10.1111/tpj.13415

Czarnecki O, Hedtke B, Melzer M, Rothbart M, Richter A, Schroter Y, Pfannschmidt T, Grimm B. An Arabidopsis GluTR binding protein mediates spatial separation of 5-aminolevulinic acid synthesis

in chloroplasts. Plant Cell. 2011:**23**(12):4476–4491. https://doi.org/10.1105/tpc.111.086421

Czechowski T, Bari RP, Stitt M, Scheible WR, Udvardi MK. Real-time RT-PCR profiling of over 1400 Arabidopsis transcription factors: unprecedented sensitivity reveals novel root- and shoot-specific genes. Plant J. 2004:**38**(2):366–379. https://doi.org/10.1111/j.1365-313X.2004.02051.x

Douce R, Joyard J. Biochemistry and function of the plastid envelope. Annu Rev Cell Biol. 1990:**6**(1):173–216. https://doi.org/10.1146/annurev.cb.06.110190.001133

Fan T, Roling L, Meiers A, Brings L, Ortega-Rodes P, Hedtke B, Grimm B. Complementation studies of the Arabidopsis fc1 mutant substantiate essential functions of ferrochelatase 1 during embryogenesis and salt stress. Plant Cell Environ. 2019:**42**(2):618–632. https://doi.org/10.1111/pce.13448

Ferro M, Brugiere S, Salvi D, Seigneurin-Berny D, Court M, Moyet L, Ramus C, Miras S, Mellal M, Le Gall S, et al. AT_CHLORO, a comprehensive chloroplast proteome database with subplastidial localization and curated information on envelope proteins. Mol Cell Proteomics. 2010:**9**(6):1063–1084. https://doi.org/10.1074/mcp.M900325-MCP200

Froehlich JE, Wilkerson CG, Ray WK, McAndrew RS, Osteryoung KW, Gage DA, Phinney BS. Proteomic study of the *Arabidopsis thaliana* chloroplastic envelope membrane utilizing alternatives to traditional two-dimensional electrophoresis. J Proteome Res. 2003:**2**(4):413–425. https://doi.org/10.1021/pr034025j

Giglione C, Fieulaine S, Meinnel T. N-terminal protein modifications: bringing back into play the ribosome. Biochimie. 2015:**114**:134–146. https://doi.org/10.1016/j.biochi.2014.11.008

Jacobs JM, Jacobs NJ, Sherman TD, Duke SO. Effect of diphenyl ether herbicides on oxidation of protoporphyrinogen to protoporphyrin in organellar and plasma membrane enriched fractions of barley. Plant Physiol. 1991:**97**(1):197–203. https://doi.org/10.1104/pp.97.1.197

Joyard J, Ferro M, Masselon C, Seigneurin-Berny D, Salvi D, Garin J, Rolland N. Chloroplast proteomics and the compartmentation of plastidial isoprenoid biosynthetic pathways. Mol Plant. 2009:**2**(6):1154–1180. https://doi.org/10.1093/mp/ssp088

Kannangara CG, Gough SP, Hansen B, Rasmussen JN, Simpson DJ. A homogenizer with replaceable razor blades for bulk isolation of active barley plastids. Carlsberg Res Commun. 1977:**42**(6):431. https://doi.org/10.1007/BF02906279

Kobayashi K, Masuda T, Tajima N, Wada H, Sato N. Molecular phylogeny and intricate evolutionary history of the three isofunctional enzymes involved in the oxidation of protoporphyrinogen IX. Genome Biol Evol. 2014:**6**(8):2141–2155. https://doi.org/10.1093/gbe/evu170

Koch M, Breithaupt C, Kiefersauer R, Freigang J, Huber R, Messerschmidt A. Crystal structure of protoporphyrinogen IX oxidase: a key enzyme in haem and chlorophyll biosynthesis. EMBO J. 2004:**23**(8):1720–1728. https://doi.org/10.1038/sj.emboj.7600189

Lee HJ, Duke SO. Protoporphyrinogen IX-oxidizing activities involved in the mode of action of peroxidizing Herbicides. J Agric Food Chem. 1994:**42**(11):2610–2618. https://doi.org/10.1021/jf00047a044

Lermontova I, Grimm B. Reduced activity of plastid protoporphyrinogen oxidase causes attenuated photodynamic damage during high-light compared to low-light exposure. Plant J. 2006:**48**(4):499–510. https://doi.org/10.1111/j.1365-313X.2006.02894.x

Lermontova I, Kruse E, Mock HP, Grimm B. Cloning and characterization of a plastidal and a mitochondrial isoform of tobacco protoporphyrinogen IX oxidase. Proc Natl Acad Sci U S A. 1997:**94**(16):8895–8900. https://doi.org/10.1073/pnas.94.16.8895

Li HM, Teng YS. Transit peptide design and plastid import regulation. Trends Plant Sci. 2013:**18**(7):360–366. https://doi.org/10.1016/j.tplants.2013.04.003

Li J, Zhang F, Li Y, Yang W, Lin R. Chloroplast-localized protoporphyrinogen IX oxidase1 is involved in the mitotic cell cycle in Arabidopsis. Plant Cell Physiol. 2019:**60**(11):2436–2448. https://doi.org/10.1093/pcp/pcz135

Matringe M, Camadro JM, Block MA, Joyard J, Scalla R, Labbe P, Douce R. Localization within chloroplasts of protoporphyrinogen oxidase, the target enzyme for diphenylether-like herbicides. J Biol Chem. 1992:**267**(7):4646–4651. https://doi.org/10.1016/S0021-9258(18)42882-7

Meskauskiene R, Nater M, Goslings D, Kessler F, op den Camp R, Apel K. FLU: a negative regulator of chlorophyll biosynthesis in *Arabidopsis thaliana*. Proc Natl Acad Sci U S A. 2001:**98**(22):12826–-12831. https://doi.org/10.1073/pnas.221252798

Miras S, Salvi D, Ferro M, Grunwald D, Garin J, Joyard J, Rolland N. Non-canonical transit peptide for import into the chloroplast. J Biol Chem. 2002:**277**(49):47770–47778. https://doi.org/10.1074/jbc.M207477200

Miras S, Salvi D, Piette L, Seigneurin-Berny D, Grunwald D, Reinbothe C, Joyard J, Reinbothe S, Rolland N. Toc159- and Toc75-independent import of a transit sequence-less precursor into the inner envelope of chloroplasts. J Biol Chem. 2007:**282**(40):29482–29492. https://doi.org/10.1074/jbc.M611112200

Mochizuki N, Tanaka R, Grimm B, Masuda T, Moulin M, Smith AG, Tanaka A, Terry MJ. The cell biology of tetrapyrroles: a life and death struggle. Trends Plant Sci. 2010:**15**(9):488–498. https://doi.org/10.1016/j.tplants.2010.05.012

Nada A, Soll J. Inner envelope protein 32 is imported into chloroplasts by a novel pathway. J Cell Sci. 2004:**117**(17):3975–3982. https://doi.org/10.1242/jcs.01265

Nielsen M, Ard R, Leng X, Ivanov M, Kindgren P, Pelechano V, Marquardt S. Transcription-driven chromatin repression of intragenic transcription start sites. PLoS Genet. 2019:**15**(2):e1007969. https://doi.org/10.1371/journal.pgen.1007969

Oñate-Sánchez L, Vicente-Carbajosa J. DNA-free RNA isolation protocols for Arabidopsis thaliana, including seeds and siliques. BMC Res Notes 2008:**1**(1): 93. http://dx.doi.org/10.1186/1756-0500-1-93

Porri A, Noguera MM, Betz M, Salinger D, Brandle F, Bowe SJ, Lerchl J, Meyer L, Knapp M, Roma-Burgos N. Can double PPO mutations exist in the same allele and are such mutants functional? Pest Manag Sci. 2022:**78**(6):2258–2264. https://doi.org/10.1002/ps.6850

Pulido P, Leister D. Novel DNAJ-related proteins in *Arabidopsis thaliana*. New Phytol 2018:**217**(2): 480–490. http://dx.doi.org/10.1111/nph.14827

Qin X, Sun L, Wen X, Yang X, Tan Y, Jin H, Cao Q, Zhou W, Xi Z, Shen Y. Structural insight into unique properties of protoporphyrinogen oxidase from Bacillus subtilis. J Struct Biol. 2010:**170**(1):76–82. https://doi.org/10.1016/j.jsb.2009.11.012

Qin X, Tan Y, Wang L, Wang Z, Wang B, Wen X, Yang G, Xi Z, Shen Y. Structural insight into human variegate porphyria disease. FASEB J. 2011:**25**(2):653–664. https://doi.org/10.1096/fj.10-170811

Richter AS, Banse C, Grimm B. The GluTR-binding protein is the heme-binding factor for feedback control of glutamyl-tRNA reductase. Elife. 2019:**8**:e46300. https://doi.org/10.7554/eLife.46300

Sambrook J. Molecular cloning: a laboratory manual. 3rd ed. Cold Spring Harbor (NY): Cold Spring Harbor Laboratory Press, 2001.

Scharfenberg M, Mittermayr L EVONR-L, Schlicke H, Grimm B, Leister D, Kleine T. Functional characterization of the two ferrochelatases in *Arabidopsis thaliana*. Plant Cell Environ. 2015:**38**(2):280–298. https://doi.org/10.1111/pce.12248

Tanaka R, Tanaka A. Tetrapyrrole biosynthesis in higher plants. Annu Rev Plant Biol. 2007:**58**(1):321–346. https://doi.org/10.1146/annurev.arplant.57.032905.105448

Tran HC, Van Aken O. Purification of leaf mitochondria from *Arabidopsis thaliana* using percoll density gradients. Methods Mol Biol. 2022:**2363**:1–12. https://doi.org/10.1007/978-1-0716-1653-6_1

Wang P, Liang FC, Wittmann D, Siegel A, Shan SO, Grimm B. Chloroplast SRP43 acts as a chaperone for glutamyl-tRNA reductase,

the rate-limiting enzyme in tetrapyrrole biosynthesis. Proc Natl Acad Sci U S A. 2018:**115**(5): E3588–E3596. https://doi.org/10.1073/pnas.1719645115

Watanabe N, Che FS, Iwano M, Takayama S, Yoshida S, Isogai A. Dual targeting of spinach protoporphyrinogen oxidase II to mitochondria and chloroplasts by alternative use of two in-frame initiation codons. J Biol Chem. 2001:**276**(23): 20474–20481. https://doi.org/10.1074/jbc.M101140200

Winter D, Vinegar B, Nahal H, Ammar R, Wilson GV, Provart NJ. An "electronic fluorescent pictograph" browser for exploring and analyzing large-scale biological data sets. PLoS One. 2007:**2**(8):e718. https://doi.org/10.1371/journal.pone.0000718

Woodson JD, Joens MS, Sinson AB, Gilkerson J, Salome PA, Weigel D, Fitzpatrick JA, Chory J. Ubiquitin facilitates a quality-control pathway that removes damaged chloroplasts. Science. 2015:**350**-(6259):450–454. https://doi.org/10.1126/science.aac7444

Zhang F, Tang W, Hedtke B, Zhong L, Liu L, Peng L, Lu C, Grimm B, Lin R. Tetrapyrrole biosynthetic enzyme protoporphyrinogen IX oxidase 1 is required for plastid RNA editing. Proc Natl Acad Sci U S A. 2014:**111**(5):2023–2028. doi:10.1073/pnas.1316183111